Original Article

Circulating miR-1 as a potential predictor of left ventricular remodeling following acute ST-segment myocardial infarction using cardiac magnetic resonance

Quanmei Ma[1], Yue Ma[1], Xiaonan Wang[1], Shanshan Li[1], Tongtong Yu[2], Weili Duan[2], Jiake Wu[2], Zongyu Wen[2], Yundi Jiao[2], Zhaoqing Sun[2], Yang Hou[1]

[1]Department of Radiology, [2]Department of Cardiology, Shengjing Hospital of China Medical University, Shenyang, China

Correspondence to: Yang Hou, MD, PhD. Department of Radiology, Shengjing Hospital of China Medical University, No. 36 Sanhao Street, Heping District, Shenyang, China. Email: houyang1973@163.com.

Background: The identification of patients with a high likelihood of left ventricular (LV) remodeling with a high-risk prognosis has critical implications for risk stratification after acute ST-segment elevation myocardial infarction (STEMI). This study aimed to evaluate the relationship between circulating miR-1 and 6-month post-infarct LV remodeling based on cardiac magnetic resonance (CMR) imaging.

Methods: A total of 80 patients with a first STEMI treated with primary percutaneous coronary intervention (PCI) who underwent CMR imaging 1 week and 6 months after STEMI were evaluated. The percentage changes of LV ejection fraction (LVEF), LV end-diastolic volume (LVEDV), LV end-systolic volume index (LVESV) at 1 week and 6 months after PCI (%ΔLVEF, %ΔLVEDV and %ΔLVESV) were calculated. miR-1 was measured using polymerase chain reaction (PCR)-based technologies in plasma samples that were collected at admission. The study group was divided into two groups based on a 10% cutoff value for the percentage of change in the LV end-diastolic volume (%ΔLVEDV): remodeling at high risk of major adverse cardiac events (MACEs) (%ΔLVEDV ≥10%, termed the LV remodeling group) and remodeling at lower risk of MACEs (%ΔLVEDV <10%, termed the non-LV remodeling group). The associations of miR-1 expression with the %ΔLVEDV, percentage change in the LV end-systolic volume (%ΔLVESV), and percentage change in the LV ejection fraction at follow-up were estimated.

Results: Twenty-two patients (27.5%) showed adverse LV remodeling, and 58 patients (72.5%) did not show adverse LV remodeling at the 6-month follow-up of CMR. The mean LVEF, LVEDV index, and LVESV index values at 1 week were 50.6%±8.2%, 74.6±12.8 mL/m^2, and 37.2±10.2 mL/m^2, respectively. Mean LVEF at follow-up (53.5%±10.6%) was increased compared with baseline (P<0.001). There were significant decreases in LVEDV index and LVESV index values at follow-up (72.0±14.9 mL/m^2 and 33.7±11.0 mL/m^2, respectively; P=0.009 and P<0.001, respectively). The expression of miR-1 at admission was positively correlated with the %ΔLVEDV (r=0.611, P<0.001) and %ΔLVESV (r=0.268, P=0.016). Receiver operating characteristic (ROC) analysis showed that miR-1 expression predicted LV remodeling with an area under the curve (AUC) value of 0.68 (95% CI: 0.56–0.78). Compared with the clinical factors of peak creatine kinase–myocardial band (CK–MB) and peak troponin T level, peak logNT-proBNP showed the highest predictive power, with an AUC value of 0.75 (95% CI: 0.64–0.84). A model including the clinical, CMR, and miR-1 factors showed greater predictive power (P=0.034) than a model including only clinical and CMR factors, with AUCs of 0.89 (95% CI: 0.80–0.95) and 0.81 (95% CI: 0.71–0.89), respectively.

Conclusions: Circulating miR-1 at admission is an independent predictor of LV remodeling 6 months after STEMI. miR-1 showed incremental value in predicting LV remodeling compared with the clinical and CMR measurements.

Keywords: Circulating microRNA; hsa-miR-1; left ventricular (LV) remodeling; myocardial infarction (MI); magnetic resonance imaging

Submitted Oct 06, 2019. Accepted for publication May 28, 2020.
doi: 10.21037/qims-19-829
View this article at: http://dx.doi.org/10.21037/qims-19-829

Introduction

The prognosis of acute myocardial infarction (AMI) is mainly determined by the extent of irreversible myocardial injury and left ventricular (LV) remodeling. LV remodeling, which is a crucial pathophysiological process involved in all forms of heart disease, is characterized by mechanical and electrical remodeling (1). LV remodeling includes alterations in myocyte biology and myocardial changes. Changes in excitation–contraction coupling and hypertrophy with the loss of myofilaments are characteristic of myocyte biology changes. Myocyte apoptosis, extracellular matrix degradation and fibrosis, LV dilation, and LV wall stress are indicative of myocardial changes (2). Ventricular remodeling is the process in which there is an expansion of a large infarct scar and subsequent regional ventricular dilatation and function changes. Post-infarct remodeling causes the highest risk of symptomatic heart failure, which is one of the most important causes of morbidity and mortality worldwide (3). Early risk stratification for LV remodeling is required to permit observation and more aggressive treatment of high-risk patients. The myocardial infarction (MI) area on cardiac magnetic resonance imaging (CMR) and brain natriuretic peptide (BNP) or N-terminal pro-brain natriuretic peptide (NT-proBNP) have been used to clinically predict LV remodeling. However, the ideal markers for predicting LV remodeling are unknown (4,5). The use of BNP to define the optimal cutoff value for predicting LV remodeling is problematic due to the considerable differences in measurement data (4), and the disadvantages of CMR include a high cost, long examination time, and lengthy data post-processing time (5). miRNAs provide novel opportunities for the identification of biomarkers and the development of novel therapeutic tools (6).

miRNAs are small molecules (19–22 nucleotides) that bind to messenger RNA (mRNA). They either initiate mRNA degradation or translational repression at the post-transcriptional level (7,8). The use of miRNAs as diagnostic biomarkers for MI has been explored in numerous experimental studies and patient cohorts in cardiovascular disease (9-12). miRNAs are important mediators for both pathophysiological adaptations in heart structure and function (13,14). miRNAs in the infarcted heart regulate numerous pathophysiological processes including cardiac cell hypertrophy, proliferation, death, neovascularization and cardiac fibrosis pathways (15-18). Acute depletion or the overexpression of miRNAs following MI may be useful in reducing ischemia-reperfusion injury, protecting against cardiac fibrosis and improving neovascularization to avoid long-term adverse remodeling and heart failure (15,19). Several studies have explored the role of circulating miRNAs in the prediction of LV remodeling and adverse clinical outcomes after AMI (20-22).

Previous research has demonstrated that miR-1 plays a pivotal and complex role in the process of LV remodeling after AMI (6,17,23). Makhdoumi *et al.* showed that miR-1 expression is regulated by the myocyte enhancer factor-2 and serum response factor. miR-1 regulates apoptosis through repression of the heat shock protein 60 (Hsp60) and heat shock protein 70 (Hsp70) in downstream pathways. Heat shock proteins have been shown to block apoptosis by inhibiting the mitochondrial death pathways at different points. Increased miR-1 causes the downregulation of multiple anti-apoptotic genes such as Hsp60, Hsp70, and B-cell lymphoma 2 (24-26). However, Stahlhut *et al.* (27) showed that miR-1 negatively regulated angiogenesis by modulating the levels of the potent angiogenic factor VegfA during the development of zebrafish. An earlier study revealed that miR-1 negatively regulated cardiomyocyte growth response by downregulating the calcium-calmodulin signaling through calcineurin to NFAT. It also negatively regulated the expression of Mef2a and Gata4, which are key transcription factors that mediate calcium-dependent changes in gene expression (28). Moreover, Valkov *et al.* demonstrated that there is a negative regulatory function of miR-1 in adult cardiac fibroblast proliferation, which is partially mediated by direct targeting of two cell cycle regulators, cyclin D2, and cyclin-dependent kinase 6 (29). However, the precise mechanisms underlying how miR-1 affects the process of LV remodeling has not been defined. CMR has been considered the gold standard for assessing LV volumes and mass (30,31). In the present study, we explored the potential prognostic capability of miR-1 in LV remodeling assessed by CMR parameters in patients with a first ST-segment elevation MI (STEMI).

Methods

Study subjects

Consecutive patients with a diagnosis of STEMI admitted to our hospital and treated with primary percutaneous coronary intervention (PCI) were prospectively enrolled from January 2018 to December 2018. STEMI was diagnosed by typical chest pain and ST-segment elevation on electrocardiogram (ECG) at admission (32). Patients were included if they were older than 18, had no earlier MI, met ECG criteria for acute STEMI, and underwent successful PCI with stent implantation within 12 h of symptom onset. CMR imaging was performed at 3–7 days (average 4.0±1.2 days) and 6 months after treatment with PCI.

The exclusion criteria included the refusal to participate, the presence of a prior MI, patients with in-hospital complications (death, reinfarction, and clinical instability), contraindications to CMR imaging, claustrophobia, incomplete CMR imaging data and poor CMR image quality. The relevant clinical history data included demographical, hemodynamics, angiographic and electrocardiographic information prospectively collected from each patient. The initial and post-procedural blood flow in the culprit vessel was graded according to the thrombolysis in myocardial infarction (TIMI) grading system in the following fashion: grade 0, no reperfusion; grade 1, low reperfusion; grade 2, partial reperfusion; and grade 3, regular perfusion (33). Written consent was obtained from all subjects studied, and the study protocol was approved by the local institutional committee for ethics on human research.

CMR imaging

Imaging was performed using a Philips 3.0T MR scanner (Ingenia, Philips Healthcare, Best, Netherlands). Two-chamber, four-chamber, and LV short-axis cine images were obtained using two-dimensional balanced steady-state free processing (2D b-SSFP). The LV short-axis covered the entire left ventricle. Patients underwent a T2 spectral adiabatic inversion recovery (SPAIR) scan to evaluate myocardial edema. Native T1 mapping scanning was performed before the contrast injection, and the modified Look-Locker inversion recovery (MOLLI) sequence was used to scan the base, middle, and apex regions. The acquisition mode was 3-(3)-3-(3)-5. Next, patients were intravenously injected with 0.2 mmol/kg gadolinium contrast agent (Omniscan, GE Healthcare, Ireland) in two injections. First, the contrast agent (0.03 mmol/kg) was injected using a power injector at a speed of 3 mL/s (34), followed by a 15-mL saline flush. The remaining contrast agent was injected at a rate of 1 mL/s and followed by a 20-mL saline flush. At the first injection, the first-pass perfusion image was acquired by a T1-weighted fast gradient-echo sequence which included three short-axis positions and one four-chamber position. An enhanced T1 mapping scan was performed 12 minutes after the contrast agent was injected, and the scanning parameters were the same as those of the native mapping. A late gadolinium enhancement (LGE) scan was performed 15–20 minutes after the first contrast injection. The phase-sensitive inversion recovery (PSIR) sequence was used to cover the entire left ventricle on the short-axis. The CMR imaging parameters are listed in *Table 1*.

Cardiac data were evaluated using CVI software (version 5.9.1, Circle Cardiovascular Imaging Inc., Calgary, AB, Canada). Cardiac function, including left ventricular ejection fraction (LVEF), left ventricular end-diastolic volume index (LVEDVI), left ventricular end-systolic volume index (LVESVI), and myocardial strain, was analyzed in cine images. The percentage of change for LVEF, LVEDV, and LVESV at 1 week and 6 months after AMI (%ΔLVEF, %ΔLVEDV, and %ΔLVESV) was calculated. The endocardial and epicardial borders were manually contoured and propagated on end-diastolic and end-systolic short-axis cine images. The deviation of the endocardial or epicardial contour was then manually corrected (35). Papillary muscles were included in the LV volumes and excluded from the mass calculations. The global myocardial strain values were then calculated automatically by the software on three cine views: the four-chamber, two-chamber, and short-axis cine CMR images covering the entire LV (36). Global radial and circumferential strain (GRS and GCS, respectively) values were measured on short-axis images, and global longitudinal strain (GLS) was measured on the vertical and horizontal long-axis images. The peak systolic strain during the entire cardiac cycle was defined as the peak positive (radial strain) or negative (circumferential and longitudinal strain) values (37). The myocardial extracellular volume (ECV) was measured by a combination of native T1 and enhanced T1 mapping. The ECV calculation formula was calculated as follows: myocardial ECV = (1 − hematocrit) × (myocardial ΔR1)/(blood ΔR1), where ΔR1 = 1/T1(pre-contrast) − 1/T1 (post-contrast), and hematocrit is the volumetric percentage of red blood cells in whole blood.

Table 1 CMR scanning parameters

Parameter	b-SSFP	T2 SPAIR	Native T1	First-pass perfusion	PSIR
Spatial resolution (mm^3)	1.25×1.25×8	0.91×0.91×8	1.2×1.2×8	1.2×1.2×8	0.91×0.91×8
FOV (mm^2)	340×340	340×340	320×320	320×320	320×320
TR (ms)	2.89	2,250	2.30	2.51	6.08
TE (ms)	1.45	80	1.05	1.15	3.00
Flip angle (°)	45	90	20	20	25
Matrix	140×143	232×179	136×134	120×120	220×159
Slice thickness (mm)	8	8	8	10	8

CMR, cardiac magnetic resonance imaging; FOV, field of view; TR, repetition time; TE, echo time; b-SSFP, balanced steady-state free processing; SPAIR, spectral adiabatic inversion recovery; PSIR, phase-sensitive inversion recovery.

The area at risk (AAR) was defined as myocardia with a signal intensity of > 2 standard deviations (SDs) above the average signal intensity in remote myocardia and expressed as a percentage of the total LV mass (38). The infarcted myocardium was defined as a range larger than the mean signal of the normal myocardial region of interest + 5 SDs on the PSIR image. The data were expressed as a percentage of the total LV mass. Microvascular obstruction (MVO) was defined as a low signal core in the MI area of the LGE image. As previously described, after STEMI revascularization, a %ΔLVEDV value of ≥10% showed a strong correlation with clinical outcomes, suggesting this criterion as the preferred CMR-based definition for post-STEMI LV remodeling (39). Accordingly, the study group was divided into two groups based on the %ΔLVEDV cutoff value of 10%: remodeling at high risk of major adverse cardiac events (MACEs) (%ΔLVEDV ≥10%, termed the LV remodeling group) and remodeling at lower risk of MACEs (%ΔLVEDV <10%, termed the non-LV remodeling group).

miR-1 expression

Whole-blood samples (3 mL per patient) were acquired by direct venous puncture into tubes containing sodium citrate immediately before PCI, 180 [interquartile range (IQR), 83–271] min after the onset of symptoms. Blood samples were centrifuged at 1,000 × *g* for 10 min. After centrifugation, the supernatant plasma was transferred into an RNase-free tube, and the plasma was stored at –80 ℃ until it was assayed. miR-1 was analyzed following the methods reported previously (40). Total RNA was isolated from frozen plasma samples (1 mL) using chloroform extraction procedures. For subsequent cDNA synthesis, RNA (400 ng) was reverse transcribed using the RevertAid First-Strand cDNA Synthesis Kit (Thermo, #K1622) following the manufacturer's instructions. The FastStart Universal SYBR Green Master (Rox) (Roche, Basel, Switzerland) mix was used for the relative quantification of miRNAs by real-time polymerase chain reaction (PCR) on a Real-Time PCR system (StepOnePlus, ABI). The cycle threshold (Ct) was defined as the fractional cycle number at which the fluorescence passed the given threshold. U6 was used as an internal reference. Blood samples from 10 normal healthy volunteers were used as the control group. Relative quantification of miRNA expression was calculated using the $2^{-\Delta\Delta Ct}$ method: ΔΔCT = ΔCT (target group) – ΔCT (control group) = $(CT_{\text{target miR-1}} - CT_{\text{target U6}}) - (CT_{\text{control miR-1}} - CT_{\text{control U6}})$. Patients were further subdivided into low and high miR-1 expression groups by the optimal cutoff value calculated by the Youden index (the highest sum of sensitivity plus specificity).

Statistical analysis

Statistical analyses were performed using SPSS software [v.22.0 (SPSS, Chicago, IL, USA] and GraphPad Prism, v.7.0 [GraphPad, San Diego, CA, USA)]. Categorical variables were presented as frequencies (percentages), normally distributed variables of the mean (SD), or as medians (IQR). Categorical variables were compared using Fisher's exact test or chi-squared test depending on the size of the categories. Student's *t*-test or analysis of variance (ANOVA) was used to compare normally distributed continuous variables if there were more than two variables. Otherwise,

the Mann–Whitney test or Kruskal–Wallis test was used. A receiver operating curve (ROC) was constructed, and the area under the curve (AUC) was calculated to assess the predictive power of miR-1 for LV remodeling. The strength of the relationship between miR-1 and routine laboratory tests and CMR measurements was evaluated using Spearman's correlation test. Based on prior medical knowledge and independent of their p value, the candidate covariates were selected. Four different models were implemented using multiple linear regression and binary logistic regression analysis: model 1 (clinical factors), model 2 (clinical and miR-1 factors), model 3 (clinical and CMR factors), and model 4 (clinical + miR-1 + CMR factors). The significance level was set at 0.05 and two-sided tests were performed.

Results

Patient characteristics

A total of 80 patients with available miR-1 measurements at 1 week and follow-up CMR at 6 months were included in the study, with 22 patients (27.5%) showing LV remodeling at follow-up CMR. Compared with the non-LV remodeling group, there were no significant differences in sex, body mass index (BMI), hypertension status, diabetes mellitus, family history of AMI, chronic obstructive pulmonary disease (COPD), or smoking history in the LV remodeling group. Compared with the non-remodeling group, the remodeling group had a higher peak creatine kinase-MB (CK-MB) level [118 (64.3–243.1) *vs.* 174.6 (120.4–343.7) U/L, P=0.039]. The remodeling group showed a larger peak troponin T level than the non-remodeling group [4.6 (IQR, 3.5–9.0) *vs.* 2.6 (IQR, 0.7–4.1) ng/mL, P=0.001]. Peak NT-proBNP levels were significantly higher in the remodeling group than in the non-remodeling group [1,125.8 (IQR, 358.1–1,825) *vs.* 203.8 (IQR, 75.2–675) pg/mL, P=0.001]. Both groups had similar cardioprotective medications and use of metformin. The demographics and clinical characteristics of the study population are presented in *Table 2*.

CMR parameters

Infarct size was significantly different between the LV remodeling and non-remodeling groups (P=0.009): 18.8% (IQR, 12.0–27.7%) *vs.* 12.6% (IQR, 7.7–18.1%), respectively. The mean LVEF, LVEDVI, and LVESVI values at 1 week were 50.6%±8.2%, 74.6±12.8 mL/m^2, and 37.2±10.2 mL/m^2, respectively. The mean LVEF at follow-up (53.5%±10.6%) was increased compared with the baseline (P<0.001). Furthermore, there were significant decreases in LVEDVI and LVESVI values at follow-up (72.0±14.9 and 33.7±11.0 mL/m^2, respectively; P=0.009 and P<0.001, respectively). Infarct size was not significantly different between the 1-week and the 6-month follow-up [13.5% (IQR, 8.3–20.3%) *vs.* 12.1% (IQR, 7.3–20.1%), P=0.098]. Of the 33 patients, 23 patients with MVO at 1 week did not show MVO at 6 months (41.2% *vs.* 12.5%, P<0.001). The %ΔLVEF, %ΔLVEDV, and %ΔLVESV were 6.1%±14.9%, 3.5% (IQR, −6.2% to 10.6%), and −9.4%±15.5%, respectively. The CMR data of the study population are presented in *Table 3*.

miR-1 expression

The expression of miR-1 was significantly different between the LV remodeling and non-LV remodeling groups (7.35±3.11 *vs.* 3.52±3.54, respectively; P<0.001) (*Figure 1*). There was a slightly positive correlation observed between miR-1 expression and peak troponin T (r=0.283, P=0.011) (*Figure 2A*). We found a weakly positive correlation of miR-1 expression with LVEDVI, infarct size, and ECV at baseline (r=0.269, 0.352, and 0.274, respectively; all P<0.05) (*Figure 2B*,*C*,*D*). The expression level of miR-1 showed no correlations with baseline LVEF (P=0.836). The expression of miR-1 at admission was positively correlated with %ΔLVEDV (r=0.611, P<0.001) (*Figure 2E*) and positively correlated with %ΔLVESV (r=0.268, P=0.016) (*Figure 2F*); however, there was no significant correlation with %ΔLVEF (P=0.652).

Predictive value of miR-1 for LV remodeling

ROC analysis showed that the expression of miR-1 predicted LV remodeling with an AUC value of 0.68 (95% CI: 0.56–0.78) (*Figure 3*). When the miR-1 cutoff value was 2.03, the sensitivity and specificity were 0.86 and 0.53, respectively. Compared with the clinical factors of peak CK-MB and peak troponin T, peak logNT-proBNP showed the greatest predictive power, with an AUC of 0.75 (95% CI: 0.64–0.84). We found no significant difference in the c-index between miR-1 and the peak logNT-proBNP for LV remodeling prediction. For CMR parameters, the infarct size was observed to have a larger AUC (0.62, 95% CI: 0.51–0.73) to predict LV remodeling than AAR, peak

Table 2 Patient characteristics

Characteristic	Total population (n=80)	Non-LV remodeling (n=58, 72.5%)	LV remodeling (n=22, 27.5%)	χ^2	P value
Age, years	55.6±10.2	55.5±10.3	56.0±10.2	–0.200	0.842
Female, n (%)	14 (17.5)	11 (18.9)	3 (13.6)	0.314	0.575
Body mass index	26.0±3.8	26.0±3.9	26.0±3.5	–0.009	0.993
Hypertension, n (%)	34 (42.5)	24 (41.4)	10 (45.5)	0.108	0.742
Diabetes mellitus	24 (30.0)	15 (25.9)	9 (40.9)	1.720	0.190
Family history for AMI, n (%)	20 (25.0)	15 (25.9)	5 (22.7)	0.084	0.772
COPD, n (%)	5 (6.3)	3 (5.2)	2 (9.1)	0.418	0.518
Current smoker, n (%)	59 (73.8)	40 (72.4)	19 (77.3)	0.195	0.659
Peak CK-MB (U/L)	140.9 (79.9–260.9)	118 (64.3–243.1)	174.6 (120.4–343.7)	–2.069	0.039
Peak troponin T (ng/mL)	3.2 (1.3–6.0)	2.6 (0.7–4.2)	4.6 (3.5–9.0)	–3.286	0.001
Peak logNT-proBNP (pg/mL)	2.5 (2.0–3.1)	2.3 (1.9–2.8)	3.0 (2.6–3.3)	–3.464	0.001
miR-1 expression	2.7 (1.2–7.1)	2.0 (1.1–5.6)	6.0 (2.6–7.4)	–2.424	0.015
miR-1 groups, n (%)				8.788	0.004
<2.03	32 (40.0)	29 (50.0)	3 (13.6)		
≥2.03	48 (60.0)	29 (50.0)	19 (86.4)		
Culprit lesion, n (%)				0.635	0.999
RCA	28 (35.0)	20 (34.5)	8 (36.4)		
LAD	38 (47.5)	27 (46.6)	11 (50.0)		
LCX	13 (16.3)	10 (17.2)	3 (13.6)		
RI	1 (1.3)	1 (1.7)	0 (0.0)		
Time from symptom onset to PPCI (min)	180 (83–271)	180 (73–270)	143 (90–271)	–0.151	0.880
Pre-interventional TIMI flow				1.090	0.872
0	62 (77.5)	46 (79.3)	16 (72.7)		
1	4 (5)	4 (6.9)	2(9.1)		
2	8 (10)	5 (8.6)	3 (13.6)		
3	6 (7.5)	3 (5.2)	1 (4.5)		
Medication prior to admission					
Aspirin	15 (18.7)	8 (13.8)	7 (31.8)	3.402	0.065
ACEI/ARB	27 (33.8)	20 (32.8)	7 (36.4)	0.051	0.821
Beta-blockers	20 (25)	15 (25.9)	5 (22.7)	0.084	0.772
Statins	23 (28.8)	15 (25.9)	8 (36.4)	0.859	0.354
Metformin	18 (22.5)	12 (20.7)	6 (27.3)	0.396	0.529

AMI, acute myocardial infarction; COPD, chronic obstructive pulmonary disease; CK-MB, creatine kinase-MB; NT-proBNP, N-terminal pro-brain natriuretic peptide; RCA, right coronary artery; LAD, left anterior descending artery; LCX, left circumflex artery; RI, ramus intermedius; PPCI, primary percutaneous coronary intervention; TIMI, Thrombolysis in Myocardial Infarction; ACEI/ARB, angiotensin-converting enzyme inhibitors and/or angiotensin receptor blockers.

Table 3 CMR measurements

Characteristic	Total population (n =80)	Non-LV remodeling (n=58, 72.5%)	LV remodeling (n=22, 27.5%)	χ^2	P value
LVEF baseline (%)	50.6±8.2	51.9±7.9	47.2.0±8.2	2.367	0.020
LVEDV baseline (mL)	135.6±22.2	136.5±19.3	133.4±28.8	0.567	0.572
LVEDVi baseline (mL/m^2)	74.6±12.8	75.1±12.2	73.1±14.5	0.614	0.541
LVESV baseline (mL)	67.6±18.2	66.1±15.9	71.5±23.2	–1.195	0.236
LVESVi baseline (mL/m^2)	37.2±10.2	36.4±9.5	39.2±11.9	–1.068	0.289
IS baseline (% of LVMM)	13.5 (8.3–20.3)	12.6 (7.7–18.1)	18.8 (12.0–27.7)	–2.613	0.009
Myocardial area at risk	28.1±9.4	26.5±8.5	32.3±10.1	–2.545	0.013
Peak GRS	21.8±5.6	21.8±5.6	21.9±5.7	–0.039	0.969
Peak GCS	–13.4 (–15.6 to –12.1)	–13.4 (–15.1 to –12.1)	–14.0 (–16.7 to –11.8)	0.212	0.832
Peak GLS	–12.6±4.2	–12.4±2.0	–13.4±2.1	2.026	0.046
Myocardial native T1 value	1353 (1303 –1409)	1355 (1305–1414)	1352 (1300 –1402)	–0.280	0.779
Myocardial ECV	35.7 (33.8–37.6)	35.0 (33.2–36.9)	36.5 (34.7–39.4)	–2.209	0.027
MVO, n (%)				4.296	0.038
MVO (–)	33 (41.3)	28 (48.3)	5 (22.7)		
MVO (+)	47 (58.8)	30 (51.7)	17 (77.3)		
%ΔLVEF (%)	6.1±14.9	7.9±14.7	1.4±14.7	0.824	0.083
%ΔLVEDV (%)	3.5 (–6.2–10.6)	–4.4 (–7.5–4.4)	12.7 (11.0–14.4)	–9.762	< 0.001
%ΔLVESV (%)	–9.4±15.5	–13.6±14.3	1.7±13.1	–4.392	< 0.001

LVEF, left ventricular ejection fraction; LVEDV, left ventricular end diastolic volume; LVEDVi, left ventricular end-diastolic volume index; LVESV, left ventricular end-systolic volume; LVESVi, left ventricular end-systolic volume index; LVMM, left ventricular myocardial mass; LVMMi, left ventricular myocardial mass index; IS, infarct size; GRS, global radial strain; GCS, global circumferential strain; GLS, global longitudinal strain; ECV extracellular volume; MVO, microvascular obstruction.

GLS, and ECV.

Multiple logistic regression analysis for LV remodeling prediction

Table 4 shows the data from the multiple logistic regression analysis with the selected clinical, CMR, and miR-1 variables. In the binary logistic regression analyses for model 1, considering clinical laboratory variables, CK-MB and logNT-proBNP were included in the multiple logistic regression analysis with a good predictive performance for LV remodeling with an AUC value of 0.80 (95% CI: 0.69–0.88). After adding the miR-1 values to the previous model, logNT-proBNP and miR-1 were included in the multiple logistic regression analysis with an AUC value of 0.83 (95% CI: 0.73–0.90). Model 2 demonstrated a similar ability as model 1 for predicting LV remodeling (P=0.360); however, it only provided an incremental value (P=0.047) compared with logNT-proBNP alone (AUC 0.75, 95% CI: 0.64–0.84). Model 4, which included clinical, CMR, and miR-1 factors, showed greater predictive power (P=0.034) than model 3, which included clinical and CMR factors, with AUCs of 0.89 (95% CI: 0.80–0.95) and 0.81 (95% CI: 0.71–0.89), respectively. When miR-1 was considered as a binary variable and logNT-proBNP and infarct size were included in the multiple logistic regression analysis, the probability of LV remodeling in model 4 in the patients with miR-1 ≥2.03 was 9.84 times that of the patients with miR-1 <2.03. A summary of the predictive capabilities of the four models is shown in *Figure 4*.

Discussion

This CMR study was performed to investigate the role

of miR-1 in predicting the outcome of STEMI patients. The key findings can be summarized as follows: (I) the expression of miR-1 correlated with the %ΔLVEDV and %ΔLVESV at 6 months; (II) the plasma levels of miR-1 at admission was an independent variable for predicting LV remodeling after adjustment of the clinical and CMR parameters; and (III) the probability of LV remodeling in patients with an miR-1 ≥2.03 was 9.84 times that of the patients with a miR-1 <2.03 after incorporating the clinical and CMR parameters. Therefore, circulating miR-1 is a potential prognostic biomarker for LV remodeling.

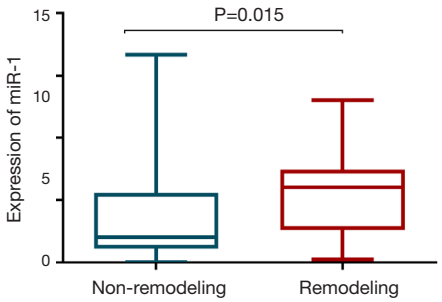

Figure 1 Circulating miR-1 expression was significantly higher in the remodeling group than in the non-remodeling group.

miR-1 was initially shown to play a role in cardiac remodeling and apoptosis-related signaling in the cellular and animal models (41-44). However, the precise role and direction of the regulation of miR-1 in the development and progression of LV remodeling and heart failure remain unknown. Previous studies have shown that miR-1 could lead to cell apoptosis by affecting anti-apoptotic genes, such as Hsp60, Hsp70, IGF-1, and Bcl-2 (2,25,44). However, miR-1 played a negative regulatory role in hypertrophy, angiogenesis and fibrosis (27,28). Adverse LV remodeling is a complicated process involving myocardial necrosis, hypertrophy, angiogenesis and fibrosis (27-29). The results showing that miR-1 is associated with %ΔLVEDV indicates that miRNAs may be functionally involved during cardiac remodeling. This is supported by the fact that infarct size was the single most important predictor of adverse ventricular remodeling (45). Elevated expression of miR-1 could indirectly indicate larger infarct size and promote

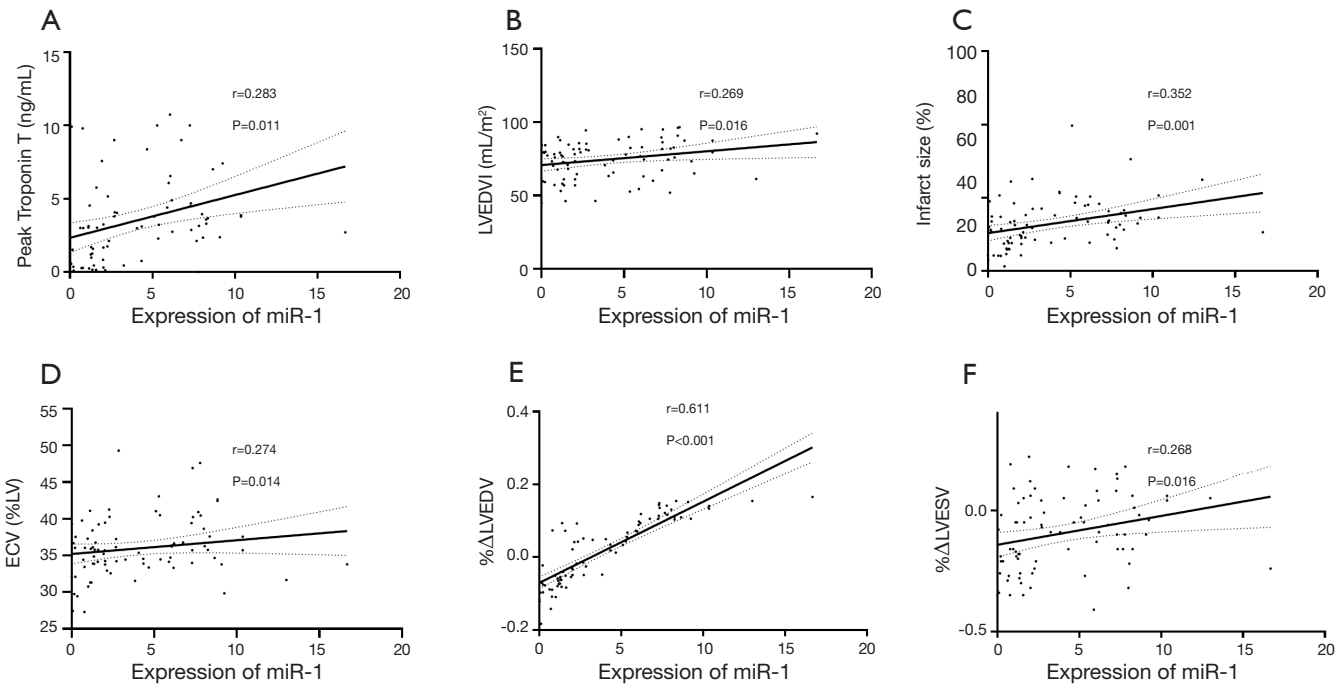

Figure 2 The association between miR-1 and CMR measurements. (A,B,C,D) The expression of miR-1 at admission was mildly correlated with peak troponin T, LVEDVI, infarct size, and ECV at baseline; (E,F) the expression of miR-1 at admission was mild to moderately correlated with the %ΔLVESV and %ΔLVEDV at 6 months. CMR, cardiac magnetic imaging; LVEDVI, left ventricular end-diastolic volume index; ECV, myocardial extracellular volume; %ΔLVEDV, the percentage change in LV end-diastolic volume; %ΔLVESV, the percentage change in LV end-systolic volume. The dashed line represents the 95% confidence intervals.

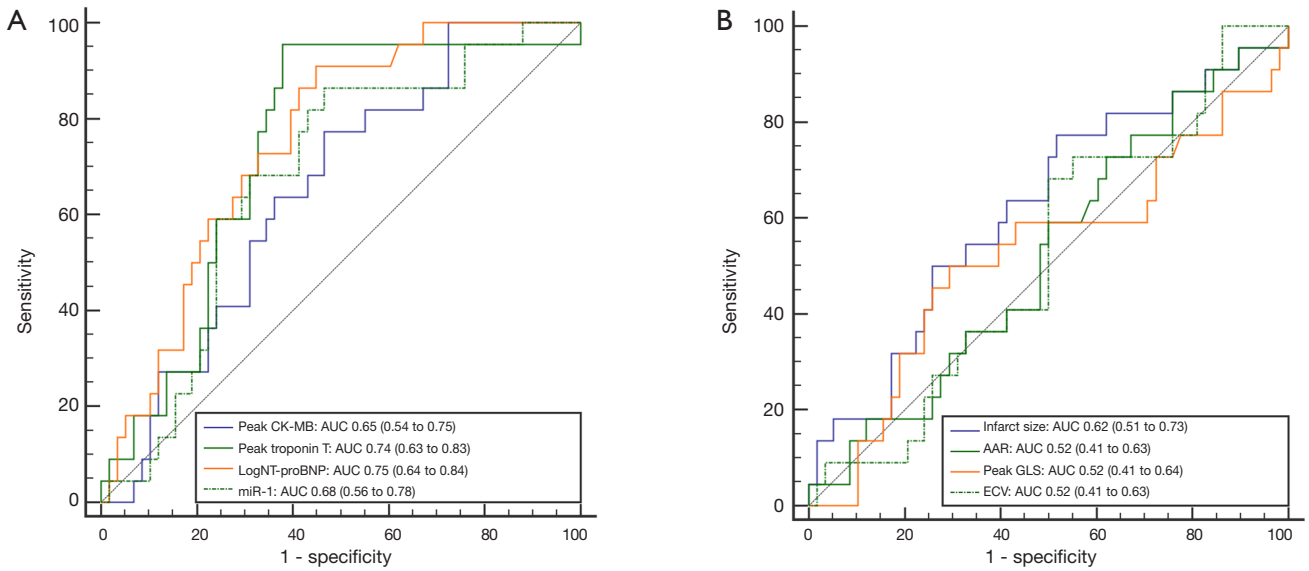

Figure 3 ROC curves of univariate variables at admission for predicting LV remodeling. (A) The AUC for miR-1 was 0.68. When the cutoff value of miR-1 was 2.03, the sensitivity and specificity were maximized at 0.86 and 0.54, respectively. The AUC for the peak CK-MB, troponin T, and logNT-proBNP were 0.65, 0.74, and 0.75, respectively; (B) The AUC for infarct size, AAR, peak GLS, and ECV were 0.62, 0.52, 0.52, and 0.52, respectively. LV, left ventricular; ROC, receiver operating characteristic; AUC, area under the curve; CK-MB, creatine kinase-MB; NT-proBNP, N-terminal pro-brain natriuretic peptide; AAR, area at risk; GLS, global longitudinal strain; ECV, extracellular volume.

more myocardial necrosis.

LV remodeling is a complex process involving cardiac myocyte growth and death, inflammation, fibrosis, neovascularization and electrophysiological remodeling involving multiple miRs (17,46). Grabmaier *et al.* (44) reported that miR-1 plasma expression levels post-AMI correlated significantly with infarct volume changes at 6 months after AMI. Zile *et al.* (47) demonstrated the upregulation of miR-1 in patients from day 2 to day 90 post-MI. These findings offer insight into the role of miR-1 as a predictive adverse ventricular remodeling marker for surrogates. However, previous research found no correlation between miR-1 and the changes in LVEDV at follow-up (44,47). These discrepant outcomes may be attributable to a variability in research cohorts and measurements (e.g., the absolute change value of LVEDV in previous work *vs.* the percentage change value of LVEDV in this study).

LV remodeling pathogenesis after acute M1 is multi-factorial, contributing to different periods spanning the moment of coronary occlusion to the development of ventricular dilatation (48). Clinical evidence suggests that post-infarct remodeling can be avoided or reversed in some instances (49); furthermore, some therapies have been demonstrated to provide great effectiveness against post-infarct remodeling. Therefore, the early identification of patients at risk of LV remodeling can have significant therapeutic benefits. We found that NT-proBNP was an independent predictive factor for LV remodeling in all the four models in our study. Comparable results have also been found in previous work (50,51). These studies illustrate the importance of specific cardiac biochemical biomarkers in predicting STEMI LV remodeling, including troponin T, CK-MB, and NT-proBNP. They found that NT-proBNP was the strongest predictor for 4-month LVEDV, likely due to the connection among LVEDV, wall pressure, and NT-proBNP. The MI area, AAR, and ECV on CMR shown in previous studies have also become important predictors of LV remodeling after infarction in AMI patients (5,52). These findings are consistent with our results. Our work showed that miR-1 provided incremental value in predicting LV remodeling compared with NT-proBNP alone and that the combination of NT-proBNP and miR-1 had a comparable performance to the clinical and CMR factors. Considering the disadvantages of CMR, which include a higher cost and longer scan and data post-processing times, our results provide a new perspective on the combination

Table 4 Multivariable-adjusted binary logistic analysis of predicting LV remodeling at 6 months

Variable	Odds ratio (95% CI)	P value
Model 1 (clinical factors)		
logNT-proBNP	6.243 (2.158–18.060)	0.001
peak CK-MB	1.004 (1.000–1.009)	0.040
Peak Troponin T	–	0.406
Model 2 (clinical + miR-1 factors)		
logNT-proBNP	6.881 (2.305–20.541)	0.001
peak CK-MB	1.005 (1.000–1.009)	0.033
Peak troponin T	–	0.173
miR-1	1.219 (1.027–1.447)	0.024
Model 3 (clinical + CMR factors)		
logNT-proBNP	5.205 (1.905–14.221)	0.001
Peak troponin T	–	0.548
peak CK-MB	–	0.090
Infarct size (%LV)	–	0.062
Area at risk (%LV)	–	0.310
GLS (%)	–	0.058
ECV (%LV)	1.171 (1.017–1.349)	0.028
Model 4 (clinical + miR-1 + CMR factors)		
logNT-proBNP	7.015 (2.058–23.915)	0.002
Peak troponin T	–	0.263
peak CK-MB	–	0.163
miR-1	1.494 (1.167–1.914)	0.001
Infarct size (%LV)	1.080 (1.005–1.161)	0.036
Area at risk (%LV)	–	0.683
GLS (%)	–	0.093
ECV (%LV)	1.333 (1.089–1.631)	0.005

NT-proBNP, N-terminal pro-brain natriuretic peptide; CK-MB, creatine kinase-MB; GLS, global longitudinal strain; LV, left ventricular; ECV, extracellular volume.

of NT-proBNP and miR-1 instead of routine CMR for LV remodeling.

This study also shows that miR-1 has a prognostic value for positive cardiac remodeling. Even after an adjustment for the relative clinical and CMR factors, the miR-1 plasma levels were still correlated with LV remodeling parameters. Our results suggest that there is potential importance in circulating miR-1, which may be used as a prognostic tool and complement relevant peptide biomarkers to identify patients with a high risk of adverse LV remodeling following acute cardiovascular events such as STEMI. Therapeutic inhibition of miRNAs in the cardiovascular field is efficient in improving cardiac outcomes in models of preclinical cardiac disease (53). Therefore, plasma miR-1 levels may be used for early therapeutic intervention.

While miR-1 shows promise as a prognostic marker, some limitations of the current study need to be considered. First, the sample size of this study is small, and further evaluation of the clinical significance of miR-1 for risk prediction of LV remodeling after AMI post-PCI is required. Second, the temporal profile of circulating miRNAs may offer better prognostic information than single measurements (46). The temporal changes in the miR-1 level in circulation at early time points (within 24 h and also 1–7 days) could be a significant challenge to the use of miR-1 in the early identification of LV changes after MI (23,40,54). Third, for this study, the decision to focus on miR-1 was based on prior research showing that miR-1 was highly associated with myocardial injury. Other miRNAs may also have prognostic value for LV remodeling, and RNA sequencing or microarray methods appear to be the basis for the identification of these additional miRNAs (20). Fourth, many reports have shown that miR-1 is related to tumors, and this study did not include cancer patients to avoid this bias (55). Fifth, the influence of medications, such as metformin, on the level of circulating miR-1 and LV remodeling deserves further investigation as emerging evidence has indicated that metformin can alter the levels of circulatory miRNAs such as miR-194-5p and miR-148-3a (56). Furthermore, it has been reported that high blood pressure, diabetes mellitus, and COPD affect LV remodeling (57-59). Although the distribution of these factors was not different between the two groups, the influence of these variables on the results of this study cannot be discounted. A method for completely controlling factors related to these variables needs to be obtained. Finally, our findings determined the relationship between miR-1 and LV remodeling, but we do not clarify the relationship between miR-1 and clinical events during long-term follow-up.

In conclusion, circulating miR-1 at admission is an independent, predictive factor of LV remodeling post-STEMI and may provide critical information for early therapeutic interventions for LV remodeling after STEMI.

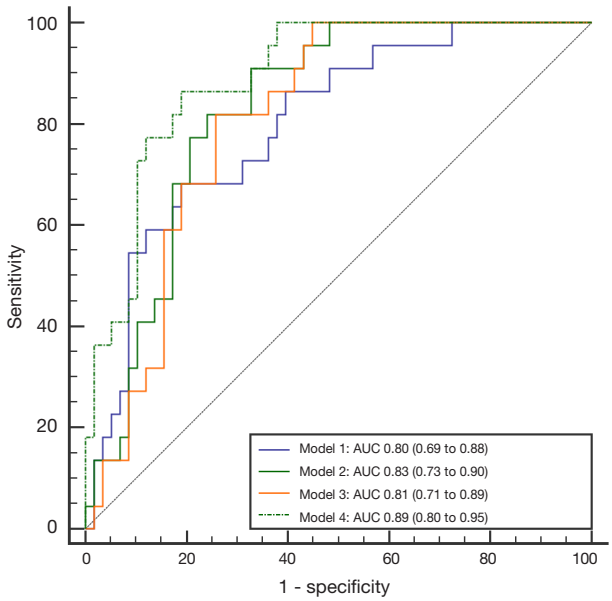

Figure 4 The ROC curve for risk prediction models. For model 1 (peak CK-MB and peak logNT-proBNP), the sensitivity and specificity were maximized at 0.68 and 0.81, respectively. For model 2 (peak CK-MB, peak logNT-proBNP, and miR-1), the sensitivity and specificity were maximized at 0.91 and 0.67, respectively. For model 3 (peak logNT-proBNP and ECV), the sensitivity and specificity were maximized at 0.81 and 0.74, respectively. For model 4 (peak logNT-proBNP, miR-1, infarct size, and ECV), the sensitivity and specificity were maximized at 0.86 and 0.81, respectively. Model 4 showed the highest predictive performance for LV remodeling (AUC 0.89, 95% CI: 0.80–0.95). ROC, receiver operating characteristic; AUC, area under the curve; LV, left ventricular; CK-MB, creatine kinase-MB; NT-proBNP, N-terminal pro-brain natriuretic peptide; AAR, area at risk; GLS, global longitudinal strain; ECV, extracellular volume.

Acknowledgments

We thank Dr. Xiangxuan Zhao for his assistance with the analysis of miR-1 expression.
Funding: This study was supported by the 345 Talent Project in Shengjing Hospital of China Medical University.

Footnote

Conflicts of Interest: All authors have completed the ICMJE uniform disclosure form (available at http://dx.doi.org/10.21037/qims-19-829). The authors have no conflicts of interest to declare.

Ethical Statement: All human experiments were performed in compliance with the institutional review board and all subjects provided informed consent for the study.

References

1. Li N, Zhou H, Tang Q. miR-133: A Suppressor of Cardiac Remodeling? Front Pharmacol 2018;9:903.
2. Topkara VK, Mann DL. Role of microRNAs in cardiac remodeling and heart failure. Cardiovasc Drugs Ther 2011;25:171-82.
3. Galli A, Lombardi F. Postinfarct Left Ventricular Remodelling: A Prevailing Cause of Heart Failure. Cardiol Res Pract 2016;2016:2579832.
4. Fertin M, Dubois E, Belliard A, Amouyel P, Pinet F, Bauters C. Usefulness of Circulating Biomarkers for the Prediction of Left Ventricular Remodeling After Myocardial Infarction. Am J Cardiol 2012;110:277-83.
5. Kim EK, Song YB, Chang SA, Park SJ, Hahn JY, Choi

SH, Choi JH, Gwon HC, Park SW, Choe YH, Ahn J, Carriere K, Lee SC. Is cardiac magnetic resonance necessary for prediction of left ventricular remodeling in patients with reperfused ST-segment elevation myocardial infarction? Int J Cardiovasc Imaging 2017;33:2003-12.
6. Poller W, Dimmeler S, Heymans S, Zeller T, Haas J, Karakas M, Leistner D-M, Jakob P, Nakagawa S, Blankenberg S, Engelhardt S, Thum T, Weber C, Meder B, Hajjar R, Landmesser U. Non-coding RNAs in cardiovascular diseases: diagnostic and therapeutic perspectives. Eur Heart J 2018;39:2704-16.
7. Schulte C, Karakas M, Zeller T. microRNAs in cardiovascular disease - clinical application. Clin Chem Lab Med 2017;55:687-704.
8. Novák J, Olejníčková V, Tkáčová N, Santulli G. Mechanistic Role of MicroRNAs in Coupling Lipid Metabolism and Atherosclerosis. Adv Exp Med Biol 2015;887:79-100.
9. Navickas R, Gal D, Laucevičius A, Taparauskaitė A, Zdanytė M, Holvoet P. Identifying circulating microRNAs as biomarkers of cardiovascular disease: a systematic review. Cardiovasc Res 2016;111:322-37.
10. Schulte C, Zeller T. microRNA-based diagnostics and therapy in cardiovascular disease-Summing up the facts. Cardiovasc Diagn Ther 2015;5:17-36.
11. Ye Y, Perez-Polo JR, Qian J, Birnbaum Y. The role of microRNA in modulating myocardial ischemia-reperfusion injury. Physiol Genomics 2011;43:534-42.
12. Wang JX, Zhang XJ, Li Q, Wang K, Wang Y, Jiao JQ, Feng C, Teng S, Zhou LY, Gong Y, Zhou ZX, Liu J, Wang JL, Li PF. MicroRNA-103/107 Regulate Programmed Necrosis and Myocardial Ischemia/Reperfusion Injury Through Targeting FADD. Circ Res 2015;117:352-63.
13. Fernandes T, Barauna VG, Negrao CE, Phillips MI, Oliveira EM. Aerobic exercise training promotes physiological cardiac remodeling involving a set of microRNAs. Am J Physiol Heart Circ Physiol 2015;309:H543-52.
14. Kumarswamy R, Thum T. Non-coding RNAs in Cardiac Remodeling and Heart Failure. Circ Res 2013;113:676-89.
15. Boon RA, Dimmeler S. MicroRNAs in myocardial infarction. Nature Reviews Cardiology 2015;12:135-42.
16. Wu K, Zhao Q, Li Z, Li N, Xiao Q, Li X, Zhao Q. Bioinformatic screening for key mi RNA s and genes associated with myocardial infarction. FEBS open bio 2018;8:897-913.
17. Zhou SS, Jin JP, Wang JQ, Zhang ZG, Freedman JH, Zheng Y, Cai L. miRNAS in cardiovascular diseases: potential biomarkers, therapeutic targets and challenges. Acta Pharmacol Sin 2018;39:1073-84.
18. Gupta SK, Foinquinos A, Thum S, Remke J, Zimmer K, Bauters C, de Groote P, Boon RA, de Windt LJ, Preissl S, Hein L, Batkai S, Pinet F, Thum T. Preclinical Development of a MicroRNA-Based Therapy for Elderly Patients With Myocardial Infarction. J Am Coll Cardiol 2016;68:1557-71.
19. Bernardo BC, Nguyen SS, Gao X-M, Tham YK, Ooi JY, Patterson NL, Kiriazis H, Su Y, Thomas CJ, Lin RC. Inhibition of miR-154 protects against cardiac dysfunction and fibrosis in a mouse model of pressure overload. Sci Rep 2016;6:22442.
20. de Gonzalo-Calvo D, Cediel G, Bar C, Nunez J, Revuelta-Lopez E, Gavara J, Rios-Navarro C, Llorente-Cortes V, Bodi V, Thum T, Bayes-Genis A. Circulating miR-1254 predicts ventricular remodeling in patients with ST-Segment-Elevation Myocardial Infarction: A cardiovascular magnetic resonance study. Sci Rep 2018;8:15115.
21. de Gonzalo-Calvo D, van der Meer RW, Rijzewijk LJ, Smit JWA, Revuelta-Lopez E, Nasarre L, Escola-Gil JC, Lamb HJ, Llorente-Cortes V. Serum microRNA-1 and microRNA-133a levels reflect myocardial steatosis in uncomplicated type 2 diabetes. Sci Rep 2017;7:47.
22. Devaux Y, Mueller M, Haaf P, Goretti ET, werenbold R, Zangrando J, Vausort M, Reichlin T, Wildi K, Moehring B, Wagner DR, Mueller C. Diagnostic and prognostic value of circulating microRNAs in patients with acute chest pain. J Int Med 2015;277:260-71.
23. Su T, Shao X, Zhang X, Han Z, Yang C, Li X. Circulating microRNA-1 in the diagnosis and predicting prognosis of patients with chest pain: a prospective cohort study. BMC Cardiovasc Disord 2019;19:5.
24. Makhdoumi P, Roohbakhsh A, Karimi G. MicroRNAs regulate mitochondrial apoptotic pathway in myocardial ischemia-reperfusion-injury. Biomed Pharmacother 2016;84:1635-44.
25. Xu C, Lu Y, Pan Z, Chu W, Luo X, Lin H, Xiao J, Shan H, Wang Z, Yang B. The muscle-specific microRNAs miR-1 and miR-133 produce opposing effects on apoptosis by targeting HSP60, HSP70 and caspase-9 in cardiomyocytes. J Cell Sci 2007;120:3045-52.
26. Tang Y, Zheng J, Sun Y, Wu Z, Liu Z, Huang G. MicroRNA-1 regulates cardiomyocyte apoptosis by targeting Bcl-2. Int Heart J 2009;50:377-87.
27. Stahlhut C, Suarez Y, Lu J, Mishima Y, Giraldez AJ. miR-1 and miR-206 regulate angiogenesis by modulating VegfA expression in zebrafish. Development (Cambridge,

England) 2012;139:4356-64.
28. Ikeda S, He A, Kong SW, Lu J, Bejar R, Bodyak N, Lee KH, Ma Q, Kang PM, Golub TR, Pu WT. MicroRNA-1 negatively regulates expression of the hypertrophy-associated calmodulin and Mef2a genes. Mol Cell Biol 2009;29:2193-204.
29. Valkov N, King ME, Moeller J, Liu H, Li X, Zhang P. MicroRNA-1-Mediated Inhibition of Cardiac Fibroblast Proliferation Through Targeting Cyclin D2 and CDK6. Front Cardiovasc Med 2019;6:65.
30. Beitner N, Jenner J, Sorensson P. Comparison of Left Ventricular Volumes Measured by 3DE, SPECT and CMR. J Cardiovasc Imaging 2019;27:200-11.
31. Liu T, Wang C, Li S, Zhao Y, Li P. Age- and gender-related normal references of right ventricular strain values by tissue tracking cardiac magnetic resonance: results from a Chinese population. Quant Imaging Med Surg 2019;9:1441-50.
32. Thygesen K, Alpert JS, Jaffe AS, Chaitman BR, Bax JJ, Morrow DA, White HD. Fourth Universal Definition of Myocardial Infarction (2018). J Am Coll Cardiol 2018;72:2231-64.
33. Chesebro JH, Knatterud G, Roberts R, Borer J, Cohen LS, Dalen J, Dodge HT, Francis CK, Hillis D, Ludbrook P. Thrombolysis in Myocardial Infarction (TIMI) Trial, Phase I: A comparison between intravenous tissue plasminogen activator and intravenous streptokinase. Clinical findings through hospital discharge. Circulation 1987;76:142-54.
34. Borlotti A, Jerosch-Herold M, Liu D, Viliani D, Bracco A, Alkhalil M, De Maria GL, Channon KM, Banning AP, Choudhury RP, Neubauer S, Kharbanda RK, Dall'Armellina E. Acute Microvascular Impairment Post-Reperfused STEMI Is Reversible and Has Additional Clinical Predictive Value: A CMR OxAMI Study. JACC Cardiovasc imaging 2019;12:1783-93.
35. Klug G, Metzler B. Assessing myocardial recovery following ST-segment elevation myocardial infarction: short- and long-term perspectives using cardiovascular magnetic resonance. Expert Rev Cardiovasc Ther 2013;11:203-19.
36. Yoon YE, Kang SH, Choi HM, Jeong S, Sung JM, Lee SE, Cho I, Cho GY, Chang HJ, Chun EJ. Prediction of infarct size and adverse cardiac outcomes by tissue tracking-cardiac magnetic resonance imaging in ST-segment elevation myocardial infarction. Eur Radiol 2018;28:3454-63.
37. Hu LW, Liu XR, Wang Q, Barton GP, Ouyang RZ, Sun AM, Guo C, Han TT, Yao XF, Francois CJ, Zhong YM. Systemic ventricular strain and torsion are predictive of elevated serum NT-proBNP in Fontan patients: a magnetic resonance study. Quant Imaging Med Surg 2020;10:485-95.
38. Schulz-Menger J, Bluemke DA, Bremerich J, Flamm SD, Fogel MA, Friedrich MG, Kim RJ, von Knobelsdorff-Brenkenhoff F, Kramer CM, Pennell DJ, Plein S, Nagel E. Standardized image interpretation and post processing in cardiovascular magnetic resonance: Society for Cardiovascular Magnetic Resonance (SCMR) board of trustees task force on standardized post processing. J Cardiovasc Magn Reson 2013;15:35.
39. Reindl M, Reinstadler SJ, Tiller C, Feistritzer HJ, Kofler M, Brix A, Mayr A, Klug G, Metzler B. Prognosis-based definition of left ventricular remodeling after ST-elevation myocardial infarction. Eur Radiol 2019;29:2330-9.
40. D'Alessandra Y, Devanna P, Limana F, Straino S, Di Carlo A, Brambilla PG, Rubino M, Carena MC, Spazzafumo L, De Simone M, Micheli B, Biglioli P, Achilli F, Martelli F, Maggiolini S, Marenzi G, Pompilio G, Capogrossi MC. Circulating microRNAs are new and sensitive biomarkers of myocardial infarction. Eur Heart J 2010;31:2765-73.
41. Thum T, Galuppo P, Wolf C, Fiedler J, Kneitz S, van Laake LW, Doevendans PA, Mummery CL, Borlak J, Haverich A, Gross C, Engelhardt S, Ertl G, Bauersachs J. MicroRNAs in the human heart: a clue to fetal gene reprogramming in heart failure. Circulation 2007;116:258-67.
42. Matkovich SJ, Van Booven DJ, Youker KA, Torre-Amione G, Diwan A, Eschenbacher WH, Dorn LE, Watson MA, Margulies KB, Dorn GW. Reciprocal regulation of myocardial microRNAs and messenger RNA in human cardiomyopathy and reversal of the microRNA signature by biomechanical support. Circulation 2009;119:1263-71.
43. He B, Jian X, Ren AJ, Zhang YF, Hao Z, Min C, Bing X, Gao XG, Wang YW. Role of miR-1 and miR-133a in myocardial ischemic postconditioning. J Biomed Sci 2011;18:22.
44. Grabmaier U, Clauss S, Gross L, Klier I, Franz WM, Steinbeck G, Wakili R, Theiss HD, Brenner C. Diagnostic and prognostic value of miR-1 and miR-29b on adverse ventricular remodeling after acute myocardial infarction - The SITAGRAMI-miR analysis. Int J Cardiol 2017;244:30-6.
45. Westman PC, Lipinski MJ, Luger D, Waksman R, Bonow RO, Wu E, Epstein SE. Inflammation as a Driver of Adverse Left Ventricular Remodeling After

Acute Myocardial Infarction. J Am Coll Cardiol 2016;67:2050-60.
46. van Boven N, Kardys I, van Vark LC, Akkerhuis KM, de Ronde MWJ, Khan MAF, Merkus D, Liu Z, Voors AA, Asselbergs FW, van den Bos E-J, Boersma E, Hillege H, Duncker DJ, Pinto YM, Postmus D. Serially measured circulating microRNAs and adverse clinical outcomes in patients with acute heart failure. Eur J Heart Fail 2018;20:89-96.
47. Zile MR, Mehurg SM, Arroyo JE, Stroud RE, DeSantis SM, Spinale FG. Relationship between the temporal profile of plasma microRNA and left ventricular remodeling in patients after myocardial infarction. Circ Cardiovasc Genet 2011;4:614-9.
48. Aboelkasem Ali Mousa M, Abdelsabour Abdallah M, Shamseddin Mohammad H, Ahmad Aly Youssef A. Early predictors of left ventricular remodeling after primary percutaneous coronary intervention. Egypt Heart J 2018;70:403-7.
49. Koitabashi N, Kass DA. Reverse remodeling in heart failure--mechanisms and therapeutic opportunities. Nat Rev Cardiol 2011;9:147-57.
50. Hendriks T, Hartman MHT, Vlaar PJJ, Prakken NHJ, van der Ende YMY, Lexis CPH, van Veldhuisen DJ, van der Horst ICC, Lipsic E, Nijveldt R, van der Harst P. Predictors of left ventricular remodeling after ST-elevation myocardial infarction. Int J Cardiovasc Imaging 2017;33:1415-23.
51. López Haldón J, Fernandez Quero M, Mancha F, Urbano JA, Guisado A, Villa M, Valle JI, Rodriguez Puras MJ, Ballesteros S, Lopez Pardo F, Diaz de la Llera L, Sanchez Gonzalez A, Martinez Martinez A. Value of NT-ProBNP level and echocardiographic parameters in ST-segment elevation myocardial infarction treated by primary angioplasty: relationships between these variables and their usefulness as predictors of ventricular remodeling. Rev Esp Cardiol 2010;63:1019-27.
52. Bulluck H, Rosmini S, Abdel-Gadir A, White SK, Bhuva AN, Treibel TA, Fontana M, Gonzalez-Lopez E, Reant P, Ramlall M, Hamarneh A, Sirker A, Herrey AS, Manisty C, Yellon DM, Kellman P, Moon JC, Hausenloy DJ. Automated Extracellular Volume Fraction Mapping Provides Insights Into the Pathophysiology of Left Ventricular Remodeling Post-Reperfused ST-Elevation Myocardial Infarction. J Am Heart Assoc 2016;5:e003555.
53. Winbanks CE, Ooi JY, Nguyen SS, McMullen JR, Bernardo BC. MicroRNAs differentially regulated in cardiac and skeletal muscle in health and disease: potential drug targets? Clin Exp Pharmacol Physiol 2014;41:727-37.
54. Schulte C, Barwari T, Joshi A, Theofilatos K, Zampetaki A, Barallobre-Barreiro J, Singh B, Sorensen NA, Neumann JT, Zeller T, Westermann D, Blankenberg S, Marber M, Liebetrau C, Mayr M. Comparative Analysis of Circulating Noncoding RNAs Versus Protein Biomarkers in the Detection of Myocardial Injury. Circ Res 2019;125:328-40.
55. Han C, Yu Z, Duan Z, Kan Q. Role of microRNA-1 in human cancer and its therapeutic potentials. Biomed Res Int 2014;2014:428371.
56. Demirsoy İH, Ertural DY, Balci S, Cinkir U, Sezer K, Tamer L, Aras N. Profiles of Circulating MiRNAs Following Metformin Treatment in Patients with Type 2 Diabetes. J Med Biochem 2018;37:499-506.
57. González A, Ravassa S, Lopez B, Moreno MU, Beaumont J, San Jose G, Querejeta R, Bayes-Genis A, Diez J. Myocardial Remodeling in Hypertension. Hypertension 2018;72:549-58.
58. Pelà G, Li Calzi M, Pinelli S, Andreoli R, Sverzellati N, Bertorelli G, Goldoni M, Chetta A. Left ventricular structure and remodeling in patients with COPD. Int J Chron Obstruct Pulmon Dis 2016;11:1015-22.
59. Yap J, Tay WT, Teng TK, Anand I, Richards AM, Ling LH, MacDonald MR, Chandramouli C, Tromp J, Siswanto BB, Investigators A-HR, Zile M, McMurray J, Lam CSP. Association of Diabetes Mellitus on Cardiac Remodeling, Quality of Life, and Clinical Outcomes in Heart Failure With Reduced and Preserved Ejection Fraction. J Am Heart Assoc 2019;8:e013114.

Cite this article as: Ma Q, Ma Y, Wang X, Li S, Yu T, Duan W, Wu J, Wen Z, Jiao Y, Sun Z, Hou Y. Circulating miR-1 as a potential predictor of left ventricular remodeling following acute ST-segment myocardial infarction using cardiac magnetic resonance. Quant Imaging Med Surg 2020;10(7):1490-1503. doi: 10.21037/qims-19-829

